Available online at www.sciencedirect.com
ScienceDirect
Journal of Sound and Vibration 319 (2009) 1312–1329
JOURNAL OF SOUND AND VIBRATION
www.elsevier.com/locate/jsvi

An expert system for predicting nonlinear aeroelastic behavior of an airfoil

C.A. Popescu[a,*], Y.S. Wong[b], B.H.K. Lee[c]

[a]Department of Mathematics and Statistics, Grant MacEwan College, 10700-104 Ave, Edmonton, Alta., Canada T5J 4S2
[b]Department of Mathematical and Statistical Sciences, University of Alberta, 632 Central Academic Building, Edmonton, Alta., Canada T6G 2G1
[c]Institute for Aerospace Research, Uplands, U-66, Ottawa, Ont., Canada K1A 0R6

Received 23 September 2007; received in revised form 24 May 2008; accepted 20 June 2008
Handling Editor: S. Bolton
Available online 5 August 2008

Abstract

In this paper we present an expert system to perform steady-state response predictions. We consider an aeroelastic model simulating a two degree-of-freedom airfoil oscillating in pitch and plunge with a freeplay nonlinearity in the pitch degree-of-freedom. In the proposed data-driven methodology, a freeplay is first confirmed, and then the locations of the switching points are determined. A state-space formulation is constructed to model the piece-wise linear system. The parameters of the system are estimated using the Kalman filter and the expectation maximization algorithm. The attractive feature of the present approach is its ability to accurately predict the steady-state behavior of the nonlinear aeroelastic system with freeplay, using only a limited amount of transient input data. To demonstrate the effectiveness of the proposed methodology, we present applications to freeplay aeroelastic data arising from wind tunnel experiments and numerical simulations.

1. Introduction

In applications of a data analysis tool to study complex engineering problems, we usually start with known measured data, and then construct a dynamical model capable of exhibiting a behavior consistent with the given data. Depending upon the problem under investigation, the dynamical model may be linear or nonlinear. Here, we propose a data-driven methodology to perform steady-state response predictions for nonlinear aeroelastic systems with freeplay.

In general, nonlinear behavior in aeroelasticity arises either from the aerodynamics or from the structure. In transonic flow regimes, the nonlinearities in aerodynamics cannot be ignored due to the presence of shock oscillations. However, in low speed regimes, linear aerodynamics is usually assumed. In the structure, nonlinearities may occur in the restoring forces, and can be classified as polynomial springs or piece-wise linear types, such as freeplay or hysteresis. Freeplay nonlinearity can occur in the control surfaces or components

*Corresponding author. Tel.: +1 7804348690; fax: +1 7804926826.
E-mail address: popescu@sirius1.math.ualberta.ca (C.A. Popescu).

0022-460X/$ - see front matter © 2008 Elsevier Ltd. All rights reserved.
doi:10.1016/j.jsv.2008.06.035

Nomenclature

$\det(\cdot)$	the determinant of a matrix
$E[\cdot]$	expected value
$E[\cdot\|\cdot]$	conditional expectation
h_N	bandwidth parameter
$K(\cdot)$	Kernel function
N	number of observations
$P(\cdot)$	probability
t	non-dimensional time
α	pitch angle
α_f	beginning of the freeplay
δ	freeplay
ξ	non-dimensional plunge displacement
$\|\cdot\|$	the absolute value of a real number

Superscript

$'$	first-order time derivative
$''$	second-order time derivative
T	transpose of a vector or matrix

with loose joints. It has been observed that even a small amount of freeplay could lead to limit cycle oscillations (LCOs) [1].

In wind tunnel experiments, it is of great importance to be able to forecast the subsequent behavior of an aircraft or control surfaces soon after the tests are initiated. Catastrophic consequences due to structural failure can be avoided if we know the possibility of encountering divergent flutter, limit-cycle oscillations, or chaotic behavior before they occur. Also, CFD/FE computations are time consuming and expensive. To be able to predict the eventual behavior of an aeroelastic system after only a few cycles of computations have been completed is highly desirable. Thus, any methodology that can predict long term behavior using a short segment of transient data is of particular interest in nonlinear aeroelasticity.

In recent years there was a growing interest to develop new data-driven steady-state prediction procedures. In Refs. [2,3] neural networks and nonlinear time series models are developed to predict the aeroelastic responses. A system identification method for predicting the aeroelastic behavior of the aircraft subjected to nonlinear aerodynamic forces is applied to simulated data in Ref. [4].

In this paper, we continue our work presented in Ref. [5], and we propose an expert system (ES) for predicting the behavior of aeroelastic systems with freeplay nonlinearities. The flowchart for the proposed ES is shown in Fig. 1. We consider an airfoil with a two degree-of-freedom (dof) motion in pitch and plunge. The freeplay is imposed in the pitch dof. If the locations of the two switching points are known, the model can be divided into a set of three linear systems. Consequently, linear system identification techniques can be

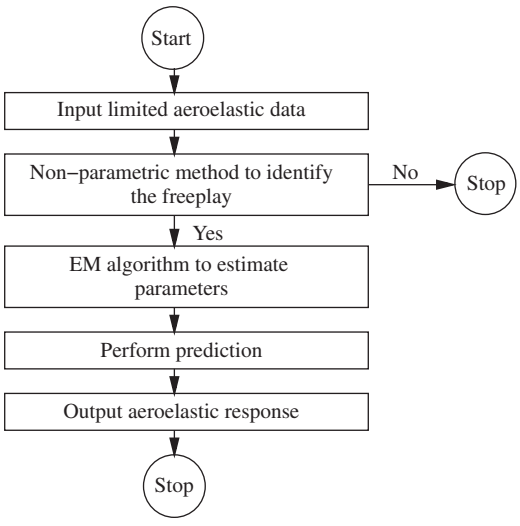

Fig. 1. Flowchart for expert system for freeplay aeroelastic prediction.

effectively applied for this particular case. Thus, the crucial step in the proposed methodology is the identification of a freeplay from the given data. Higher order spectral analysis is a popular method for detecting the nonlinear structure of aeroelastic data [6–9]. However, the bispectral methods are useful mainly to detect polynomial nonlinearities. To determine the presence and the parameters of a freeplay nonlinearity, we propose a different approach based on non-parametric estimations. If a freeplay is not detected, the procedure is terminated. Otherwise, the locations of the two switching points are determined and the aeroelastic model is represented by a discrete switching state-space system. The linear Kalman filter and the expectation–maximization (EM) algorithms are employed to estimate the parameters of the system. Predictions of the steady-state response of the aeroelastic system can then be carried out.

To illustrate the proposed approach, examples of short time duration experimental and numerically simulated aeroelastic data used as the input of the ES are shown in Fig. 2. The data "a", "b" and "c" represent the time histories of the pitch motion measured from experiments, whereas "d" is the pitch time history generated from numerical simulation. It is difficult to forecast the long term aeroelastic behavior using only the information given in this figure. From the short duration time series a simple guess suggests that for "a" the amplitude will continue to increase leading to divergence; for "b", the damped oscillations will eventually give a steady non-oscillating solution; and for both "c" and "d", the oscillations will continue with a constant amplitude leading to LCOs. However, the aeroelastic responses actually turn out to be a LCO for "a", a section of a LCO before reaching a steady non-oscillating state for "b", a steady non-oscillating solution for "c", and a divergent oscillation for "d". Using the proposed expert system it will be demonstrated that the steady-state behavior for all these cases can be correctly predicted from the short time segment given in Fig. 2.

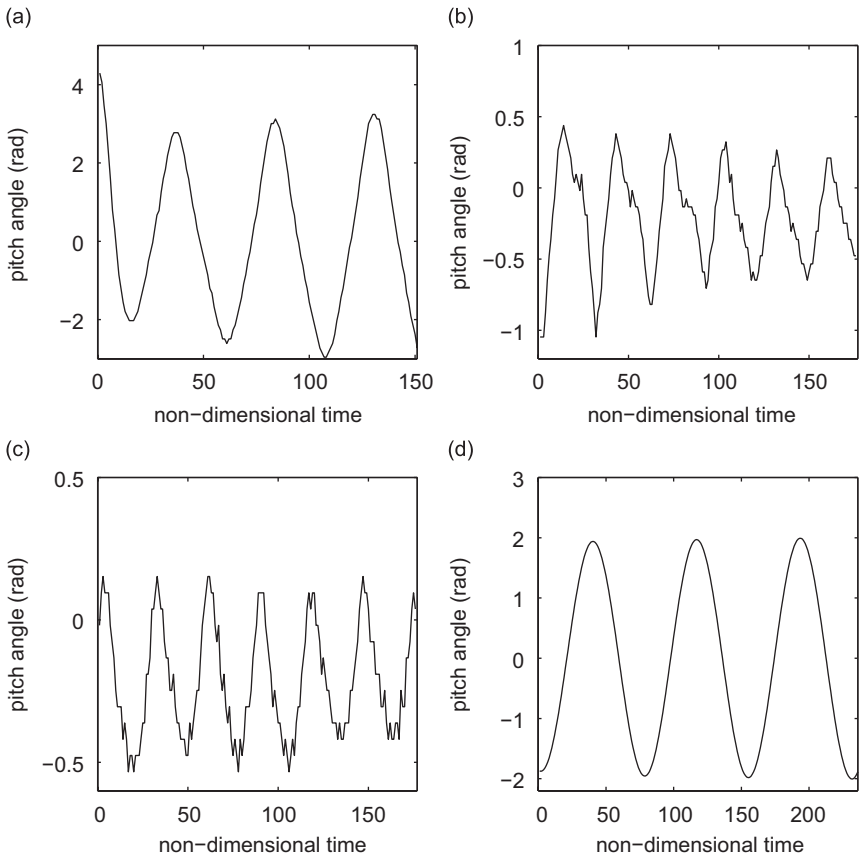

Fig. 2. Samples of input data for the expert system representing: (a) limit cycle oscillation, (b) damped signal, (c) damped signal and (d) divergent oscillations.

2. The aeroelastic model

Consider a two-dimensional aeroelastic system modeling an airfoil oscillating in pitch and plunge. The mathematical formulation can be expressed by the following coupled system of equations:

$$\xi'' + x_\alpha \alpha'' + 2\zeta_\xi \frac{\tilde{\omega}}{U^*}\xi' + \left(\frac{\tilde{\omega}}{U^*}\right)^2 G(\xi) = -\frac{1}{\pi\mu} C_L(t) \tag{1}$$

$$\frac{x_\alpha}{r_\alpha^2}\xi'' + \alpha'' + 2\frac{\zeta_\alpha}{U^*}\alpha' + \frac{1}{U^{*2}} M(\alpha) = \frac{2}{\pi\mu r_\alpha^2} C_M(t), \tag{2}$$

where x_α, r_α, ζ_α, ζ_ξ, $\tilde{\omega}$, U^*, μ are airfoil parameters, and they are defined in [10]. The nonlinear plunge and pitch stiffness terms are denoted by $G(\xi)$ and $M(\alpha)$. Here, we assume the flow is in the low speed regime, and the lift and pitching moment coefficients $C_L(t)$, $C_M(t)$ can be expressed analytically using the Wanger functions [10]. By introducing four new variables ω_1, ω_2, ω_3, ω_4, the integro-differential system (1)–(2) can be rewritten as a system of 8 nonlinear ordinary differential equations:

$$\mathbf{X}_t' = \mathbf{A}\mathbf{X}_t + \mathbf{F}(\mathbf{X}_t), \tag{3}$$

where $\mathbf{A}$ is a matrix containing the system coefficients, $\mathbf{F}$ is a nonlinear function, and $\mathbf{X}_t$ is a vector which is a function of time, and we have $\mathbf{X}_t = [\alpha, \alpha', \xi, \xi', \omega_1, \omega_2, \omega_3, \omega_4]^{\mathrm{T}}$. The expressions for $C_L(t)$, $C_M(t)$ and the derivation of the complete system can be found in Ref. [10].

In this study, we consider linear aerodynamics because the free stream velocity is assumed to be low. We impose the structural nonlinearity only in the pitch dof. Common examples of structural nonlinearities are springs with freeplay or cubic restoring forces. For freeplay the pitch stiffness term is defined by

$$M(\alpha) = \begin{cases} \alpha - \alpha_f & \text{if } \alpha < \alpha_f, \\ 0 & \text{if } \alpha_f \leqslant \alpha \leqslant \alpha_f + \delta, \\ \alpha - \alpha_f - \delta & \text{if } \alpha > \alpha_f + \delta, \end{cases} \tag{4}$$

and for cubic nonlinearity, $M(\alpha)$ is given by

$$M(\alpha) = a_3\alpha^3 + a_2\alpha^2 + a_1\alpha + a_0. \tag{5}$$

In Fig. 3, we illustrate the general behavior of these two types of nonlinearities. We notice that an important feature of a freeplay nonlinearity is the existence of two switching points. The aeroelastic model can be divided into three regions separated by the locations of the switching points. Different linear systems apply in each region, so that using Eq. (3) in Eq. (4), the model for the aeroelastic system with freeplay can be

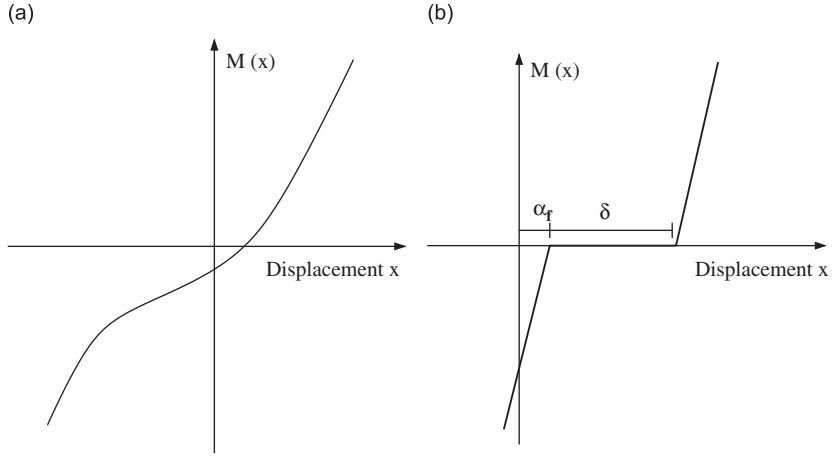

Fig. 3. General sketch for structural nonlinearities: (a) cubic spring and (b) freeplay.

written as

$$\begin{cases} \mathbf{X}_t' = \mathbf{A}\mathbf{X}_t + \mathbf{F}_1 & \text{if } X_t(1) < \alpha_f, \\ \mathbf{X}_t' = \mathbf{B}\mathbf{X}_t + \mathbf{F}_2 & \text{if } \alpha_f \leqslant X_t(1) \leqslant \alpha_f + \delta, \\ \mathbf{X}_t' = \mathbf{A}\mathbf{X}_t + \mathbf{F}_3 & \text{if } X_t(1) > \alpha_f + \delta, \end{cases} \tag{6}$$

where $X_t(1) = \alpha$ is the first component of the 8-dof vector $\mathbf{X}_t$. Here, $\mathbf{A}$ and $\mathbf{B}$ are 8×8 matrices, and $\mathbf{F}_i$, $i = 1, 2, 3$ are eight-dimensional vectors.

The corresponding discrete formulation can be written as

$$\begin{cases} \mathbf{x}_{k+1} = \mathbf{A}_1(\tau)\mathbf{x}_k + \mathbf{b}_1(\tau) & \text{if } x_k(1) < \alpha_f, \\ \mathbf{x}_{k+1} = \mathbf{A}_2(\tau)\mathbf{x}_k + \mathbf{b}_2(\tau) & \text{if } \alpha_f \leqslant x_k(1) \leqslant \alpha_f + \delta, \\ \mathbf{x}_{k+1} = \mathbf{A}_3(\tau)\mathbf{x}_k + \mathbf{b}_3(\tau) & \text{if } x_k(1) > \alpha_f + \delta, \end{cases} \tag{7}$$

where τ is a sufficiently small time step, $t = k\tau$, $\mathbf{A}_i$, $i = 1, 2, 3$ are 8×8 matrices, $\mathbf{A}_3 = \mathbf{A}_1$, and $\mathbf{b}_i$, $i = 1, 2, 3$ are eight-dimensional vectors.

3. Identification of the freeplay nonlinearity

Since our focus is on the identification of the freeplay nonlinearity, we consider a time-domain non-parametric method proven to be especially useful in the study of piece-wise linear models.

To estimate the regression curve $m(x) = E[Y|X = x]$ using a set of observations $\{(X_i, Y_i), i = 1, \ldots, N\}$, if repeated observations Y_i at $X = x$ are available, a simple solution would be to average these values. Unfortunately, this may not be applicable to aeroelastic data, if the information is given by the transient state. Nevertheless, if the function $m(x)$ is sufficiently smooth, then the values Y_i for which X_i is close to x provide good approximations of $m(x)$. Thus, instead of using a simple averaging, we consider a weighted average approach with smaller weights for Y_i with X_i far away from x, and larger weights for Y_i with X_i close to x:

$$\hat{m}(x) = \frac{1}{N}\sum_{i=1}^{N} w_i(x)\, Y_i. \tag{8}$$

The weights w_i are represented using a kernel $K(\cdot)$ which describes the shape, and a bandwidth parameter h_N which adjusts the size of the weights near x. The kernel is usually a continuous probability density function: $K(u) \geqslant 0$, and $\int K(u)\,\mathrm{d}u = 1$. The Naadaraya–Watson estimator [11] was developed based on this idea, and the general form is given by

$$\hat{m}(x) = \sum_{i=1}^{N} Y_i K_N(x - X_i) \Big/ \sum_{i=1}^{N} K_N(x - X_i), \tag{9}$$

where $K_N(u) = h_N^{-1} K(u/h_N)$. Comparing Eqs. (8) and (9), we note that the weights w_i sum to N and $\hat{m}(x)$ is adaptive to the local intensity of the X variable. The consistency of the Naadaraya–Watson estimator (i.e. the convergence of $\hat{m}(x)$ to $m(x)$ as $n \to \infty$) can be proved under reasonable assumptions [11].

Many possible kernels $K(\cdot)$ can be used in Eq. (9), but the choice is usually limited due to theoretical and practical considerations. For example, computational requirements may restrict to kernels that are zero

Table 1
Kernel functions

Kernel	$K(u)$
Triangle	$(1 - \lvert u\rvert) I_{[-1,1]}(u)$
Epanechnicov	$3(1 - u^2) I_{[-1,1]}(u)/4$
Gaussian	$\exp(-u^2/2)/\sqrt{2\pi}$

outside a certain interval. Table 1 presents three commonly used kernels which have been studied in Ref. [12] for the density estimation. The triangular and the Epanechnikov kernels are expressed in terms of the indicator function $I_{[-1,1]}(\cdot)$, and they are zero outside the interval $[-1,1]$. The Gaussian kernel is a continuous and differentiable function.

Kernel functions can be rescaled so that the differences between the estimates corresponding to different kernels are negligible [12]. Hence, by rescaling the bandwidth instead of changing the kernel functions, the choice of the kernel is not critical in practical implementations. However, the selection of the bandwidth parameter h_N is important for the interpretation of $\hat{m}(x)$. The value of h_N can be chosen automatically using the leave-on-out cross-validation method [13]. In some cases, a subjective choice of h_N is more desirable. For instance, if our interest is on the local structures, then a slightly under-smoothed curve resulting from a smaller bandwidth may be more appropriate. On the other hand, increasing the bandwidths will lead to over-smoothed curves, and subsequently to an increase in the signal-to-noise ratio.

Non-parametric methods are used to determine the thresholds for self-exciting threshold autoregressive models (SETAR) [14]. Let $\{t_0, t_1, \ldots, t_l\}$ denote the thresholds, i.e., a linearly ordered subset of real numbers, such that $t_0 < t_1 < \cdots < t_l$, $t_0 = -\infty$ and $t_l = +\infty$. A SETAR $(l; p, \ldots, p)$, where p is repeated l times, is a univariate time series $\{X_n\}$ of the form

$$X_n = a_0^{(j)} + \sum_{i=1}^{p} a_i^{(j)} X_{n-i} + e_n, \quad t_{j-1} < X_{n-d} \leqslant t_j, \tag{10}$$

for $j = 1, 2, \ldots l$, where d is a fixed integer belonging to $\{1, 2, \ldots, p\}$, and $\{e_n\}$ is a Gaussian, independent, identically distributed white noise sequence. If for $j = 1, 2, \ldots, l$, we have $a_i^{(j)} = 0$ for $i = p_j + 1, p_j + 2, \ldots, p$, then $\{X_n\}$ is known as a SETAR$(l; p_1, p_2, \ldots, p_l)$ model. Hence, a SETAR$(1, p)$ model is equivalent to a linear autoregressive model of order p.

By defining the vector $\mathbf{Y}_n = (X_n, \ldots, X_{n-p+1})^{\mathrm{T}}$, a SETAR$(l; p, p, \ldots, p)$ model can be rewritten in the following form:

$$\mathbf{Y}_n = \mathbf{f}(\mathbf{Y}_{n-1}) + \mathbf{E}_n, \tag{11}$$

where $\mathbf{E}_n = (e_n, 0, \ldots, 0)^{\mathrm{T}}$, $\mathbf{f}(\mathbf{Y}_{n-1}) = (h(\mathbf{Y}_{n-1}), X_{n-1}, \ldots, X_{n-p+1})^{\mathrm{T}}$, and $h(\mathbf{Y}_{n-1})$ is given in the right-hand side of Eq. (10).

The crucial task when working with SETAR models is to determine the thresholds and the delay parameter d. Tong [14] suggests the use of a non-parametric lag regression estimation. If $m_j(x) = E[X_n | X_{n+j}]$, replacing in Eq. (9) a non-parametric kernel estimate $\hat{m}_j(x)$ for $m_j(x)$ is

$$\hat{m}_j(x) = \sum_{i=-j+1}^{N} X_i K_N(x - X_{i+j}) \Bigg/ \sum_{i=-j+1}^{N} K_N(x - X_{i+j}), \tag{12}$$

for $j = -s, \ldots, -1$, where s is a positive integer much smaller than the size of the data set N (see Refs. [13,14]). The triangular kernel given in Table 1 is employed in Ref. [14], where

$$K_N(u) = \begin{cases} (1 - |u|/h_N)/h_N & \text{if } |u| \leqslant h_N, \\ 0 & \text{otherwise.} \end{cases} \tag{13}$$

A similar formula can be written for the non-parametric estimates $\hat{v}_j(x)$ of the variance $v_j(x) = \mathrm{VAR}(X_n | X_{n+j})$. The thresholds and the delay parameter d can be determined by analyzing the plots of $\hat{m}_j(x)$ and $\hat{v}_j(x)$ for various values of j.

The above discussion focuses on the non-parametric procedure for estimating the thresholds and delay parameters of SETAR models. However, this procedure is closely related to the present study. Obviously there are many similarities among the state-space formulations arising from the SETAR models and the aeroelastic models with freeplay. Recall that according to the locations of the switching points, the aeroelastic model with freeplay can be divided into three regions, and each region is governed by a different linear system as shown in Eq. (7). Hence, both models exhibit the common piece-wise linear characteristic, in which the changes depend on the values of the thresholds and delay parameters for the SETAR models, and on the switching points for the aeroelastic models with freeplay. Thus, by using a non-parametric estimation procedure to identify the

existence of the switching points, we can effectively confirm the presence of the freeplay nonlinearity for a given set of aeroelastic data.

4. Parameter estimation

The EM algorithm [15] is a powerful tool for parameter estimation. This algorithm is a classical method for estimating the parameters of linear systems [16], and it is particularly effective when dealing with incomplete or missing data. For a general nonlinear dynamical system, the EM algorithm has been applied using the extended Kalman filter for smoothing [17], and it has been employed in conjunction with neural networks [18].

The EM algorithm is especially useful when it is straightforward to compute the likelihood of the model using not only the observed data $\mathbf{Y}_{\text{obs}}$, but also some hidden data $\mathbf{Y}_{\text{hid}}$. In the present study, although only the pitch angle and the plunging displacement are measured, their derivatives are also present in the aeroelastic model. The EM algorithm is implemented by a data augmentation scheme, such that the observed data are a mapping of the augmented data $\mathbf{Y}_{\text{obs}} = \mathfrak{m}(\mathbf{Y}_{\text{aug}})$, where $\mathbf{Y}_{\text{aug}} = \{\mathbf{Y}_{\text{obs}}, \mathbf{Y}_{\text{hid}}\}$. The algorithm starts with an initial guess θ_0 for the unknown parameters and iteratively improve the estimation θ^*. At each iteration, the EM algorithm consists of two steps: the expectation (E) step which computes the expectation of the likelihood; and the maximization (M) step which computes the updated estimations of the parameters by maximizing the results obtained in the E-step.

More precisely, using the current estimation θ_n of the parameters, the E-step computes the conditional expectation of the augmented data log-likelihood $Q(\theta|\theta_n) = E[\log p(\theta|\mathbf{Y}_{\text{aug}})|\ \mathbf{Y}_{\text{obs}}, \theta_n]$. An approximation may be required during the E-step. In order to justify the convergence, it is important to note that the negative of the free-energy is maximized [15] with respect to the distribution component:

$$Q_{n+1} = \arg\max_{Q} \mathfrak{F}(Q, \theta_n), \tag{14}$$

where

$$\mathfrak{F}(Q, \theta) = \int Q(\mathbf{Y}_{\text{hid}}) \log p(\theta|\mathbf{Y}_{\text{aug}})\, \mathrm{d}\mathbf{Y}_{\text{hid}} - \int Q(\mathbf{Y}_{\text{hid}}) \log Q(\mathbf{Y}_{\text{hid}})\, \mathrm{d}\mathbf{Y}_{\text{hid}}. \tag{15}$$

The M-step performs maximization with respect to the parameters θ:

$$\theta_{n+1} = \arg\max_{\theta} Q(\theta|\theta_n). \tag{16}$$

In term of $\mathfrak{F}$, the M-step can be expressed as

$$\theta_{n+1} = \arg\max_{\theta} \mathfrak{F}(Q_{n+1}, \theta). \tag{17}$$

Hence, an approximation can be used in either the E-step or the M-step as long as $\mathfrak{F}$ is increasing.

An attractive feature of the EM-algorithm for parameter estimation is the guaranteed convergence [15,19]. However, depending on the initial guess, the algorithm may only converge to a local maximum. Various strategies for choosing the initial guess are proposed in Ref. [20], and techniques for accelerating the convergence are reported in Ref. [21].

We recall that for an oscillating airfoil with a freeplay nonlinearity, the mathematical formulation can be expressed by the set of linear systems given in Eq. (7). Since only α and ξ are observed in practice, Eq. (7) can be rewritten as a linear discrete switching state-space system:

$$\begin{cases} \mathbf{x}_{k+1} = \mathbf{A}_{S_{k+1}}\mathbf{x}_k + \mathbf{b}_{S_{k+1}} + \mathbf{v}_{k+1}, \\ \mathbf{y}_k = \mathbf{C}\mathbf{x}_k + \mathbf{w}_k, \end{cases} \tag{18}$$

where S_{k+1} is a discrete random variable given by

$$S_{k+1} = \begin{cases} 1 & \text{if } x_k(1) < \alpha_f, \\ 2 & \text{if } \alpha_f \leqslant x_k(1) \leqslant \alpha_f + \delta, \\ 3 & \text{if } x_k(1) > \alpha_f + \delta, \end{cases} \tag{19}$$

where A_i and b_i, $i=1,2,3$ are defined in Eq. (7), $\mathbf{y}_k=[\alpha,\xi]_k^{\mathrm{T}}$ is the two-dimensional observation vector, $\mathbf{x}_k=[\alpha,\alpha',\xi,\xi',\omega_1,\omega_2,\omega_3,\omega_4]_k^{\mathrm{T}}$ is the eight-dimensional state vector, $\mathbf{v}_k\sim N(\mathbf{0},\mathbf{Q}_{S_k})$ and $\mathbf{w}_k\sim N(\mathbf{0},\mathbf{R})$ are independent Gaussian white noise vectors, $\mathbf{Q}_i$, $i=1,2,3$ are 8×8 matrices, $\mathbf{R}$ is a 2×2 matrix, and $\mathbf{C}$ is the 2×8 matrix

$$\mathbf{C}=\begin{bmatrix}1 & 0 & 0 & \dots & 0\\ 0 & 1 & 0 & \dots & 0\end{bmatrix}. \tag{20}$$

Once α_f and δ are estimated using the non-parametric method presented in the previous section, the values of the switching variable S_k are known. Moreover, we assume that when $S_1=i$, we have $\mathbf{x}_1\sim N(\boldsymbol{\mu}_i,\boldsymbol{\Sigma}_i)$, for $i=1,2,3$. Hence, the unknown parameters of the previous model are $\theta=\{\mathbf{A}_i,\mathbf{b}_i,\mathbf{Q}_i,\mathbf{R},\boldsymbol{\mu}_i,\boldsymbol{\Sigma}_i,\ i=1,2,3\}$.

We now summarize the steps in the EM algorithm for estimating the parameters θ. First, the data is augmented with the hidden variables α', ξ', ω_1, ω_2, ω_3, ω_4 which are included in the state variables $\mathbf{x}_i$, $i=1,\dots,N$, and the complete log-likelihood $\log(L)=\log P(\mathbf{x}_1,\dots,\mathbf{x}_N,\mathbf{y}_1,\dots,\mathbf{y}_N,S_1,\dots,S_N)$ is computed. Then, the EM algorithm iteratively maximizes $\hat{E}=E[\log(L)|\mathbf{y}_1,\dots,\mathbf{y}_N,S_1=i_1,\dots,S_n=i_n]$, which can be expressed in terms of the smoothed values $\mathbf{P}_n=E[\mathbf{x}_n\mathbf{x}_n^{\mathrm{T}}|\mathbf{y}_1,\dots,\mathbf{y}_N]$, $\mathbf{P}_{n,n-1}=E[\mathbf{x}_n\mathbf{x}_{n-1}^{\mathrm{T}}|\mathbf{y}_1,\dots,\mathbf{y}_N]$, and $\mathbf{x}_{n|N}=E[\mathbf{x}_n|\ \mathbf{y}_1,\dots,\mathbf{y}_N]$. In the E-step, $\mathbf{P}_n$, $\mathbf{P}_{n,n-1}$ and $\mathbf{x}_{n|N}$ are estimated using the Kalman filtering and smoothing algorithms [16]. For the M-step, analytical updating equations for the parameters θ can be derived by taking the derivatives with respect to the parameters θ in the formula for $\hat{E}$. For completeness, the log-likelihood and the updating formulas are given in Appendix A.

The complexity of the parameter estimation process depends on the number of unknown parameters θ. For a matrix of order eight, there are 64 unknown coefficients to be estimated. Notice that in $\mathbf{x}_k=[\alpha,\alpha',\xi,\xi',\omega_1,\omega_2,\omega_3,\omega_4]_k^{\mathrm{T}}$, only the first four are physical variables, and the remaining four are introduced to eliminate the integral formulations from the aerodynamic terms. Hence, for the two-dof pitch and plunge motion of an airfoil it is reasonable to consider a reduced model with $\mathbf{x}_k=[\alpha,\alpha',\xi,\xi']_k^{\mathrm{T}}$, and α', ξ' as the only hidden variables. Using this model, the number of the unknown parameters is greatly reduced. For a matrix of order four, 16 unknown coefficients need to be determined. From the results to be presented in the case studies (Section 5), we will see that the reduced system is as effective as the full model in predicting the aeroelastic behavior.

The techniques presented in this paper can be extended to the three-dof aeroelastic models. The governing equations for a three-dof aeroelastic system with a freeplay control surface can be written as the set of 12 nonlinear ordinary differential equations derived in Ref. [22]. The non-parametric method has been tested to data arising from the three-dof system, and the freeplay nonlinearity and the locations of the switching points were successfully identified [23]. For the steady-state response prediction, the EM algorithm can still be applied as long as the associated mathematical model can be expressed in a state-space form (see Refs. [17,18] for applications regarding general nonlinear systems). However, a similar reduced model for the three-dof aeroelastic problems has not been attempted.

5. Case studies

To identify the freeplay structural nonlinearity, we apply the non-parametric method presented in Section 3. This technique has been tested for data generated from wind tunnel experiments and numerical simulations [5].

Table 2
Case studies: numerically simulated data

Pitch	Plunge	ζ_α	ζ_ξ
Freeplay, $\alpha=0.2$, $\delta=0.4$	Linear, $G(\xi)=\xi$	0	0
Freeplay, $\alpha=0.2$, $\delta=0.4$	Linear, $G(\xi)=\xi$	0.1	0.1
Freeplay, $\alpha=0.25$, $\delta=0.5$	Linear, $G(\xi)=\xi$	0	0
Freeplay, $\alpha=0.25$, $\delta=0.5$	Cubic, $G(\xi)=3\xi^3+\xi$	0	0
Freeplay, $\alpha=0.25$, $\delta=0.5$	Cubic, $G(\xi)=0.3\xi^3+\xi$	0	0
Freeplay, $\alpha=0.4$, $\delta=0.25$	Linear, $G(\xi)=\xi$	0.0154	0.0109

Table 2 lists six cases in which a freeplay is imposed in the pitch dof, and linear or cubic springs are imposed in the plunge dof. These data are simulated numerically using Eq. (3), and they are corrupted with additive Gaussian white noise with a signal-to-noise ratio of five. The results of the non-parametric method are best illustrated by analyzing the plots of the non-parametric estimates $\hat{m}_j$ against the pitch angle, for various values of j.

Fig. 4 shows the estimated mean plots for the last case listed in Table 2, i.e. a freeplay in pitch with $\alpha_f = 0.4$, $\delta = 0.25$, and the model has non-zero damping coefficients $\zeta_\alpha = 0.0154$ and $\zeta_\xi = 0.0109$. We note that initially the estimated conditional means (corresponding to $j = -1, -2, -3$) can be approximated by straight lines. As the values of j decrease, the conditional mean can no longer be represented by a straight line. The bending becomes more noticeable and the estimated conditional mean resembles the letter "Z" or its mirror image. When $j = -18$ or $j = -22$, (see Fig. 4(b),(c)) we clearly observe two extreme values near 0.4 and 0.65, and the locations of these extremes correspond to the switching points α_f and $\alpha_f + \delta$ in the aeroelastic model. Since we can identify two switching points, we conclude that the aeroelastic data is associated with a freeplay. In this case, the locations of the switching points $\alpha_f = 0.4$, $\delta = 0.25$ are determined exactly.

Based on results from many simulations with various signal-to-noise ratios, we can conclude that the non-parametric method is robust to the presence of noise. To illustrate this, we present the results obtained for the noisy data displayed in Fig. 5a. These data correspond to an aeroelastic system with a freeplay in pitch with $\alpha_f = 0.25$ and $\delta = 0.5$. We have added Gaussian white noise such that the signal-to-noise ratio is three. The system has zero damping coefficients, the non-dimensional linear fluter speed $U_L^* = 6.2851$, and the non-dimensional free stream velocity $U^* = 0.3U_L^*$, corresponding to the chaotic case investigated in Ref. [24]. The chaotic motion is shown by the "two-well potential" phase-trajectory in the α–α' plane displayed in Fig. 5b. In Fig. 6 we present the non-parametric estimates $\hat{m}_j$, for $j = -4, -11$, and -12, plotted against the pitch angle. The figures are similar to those displayed in Fig. 4. We can identify two switching points located at $\alpha_f = 0.25$

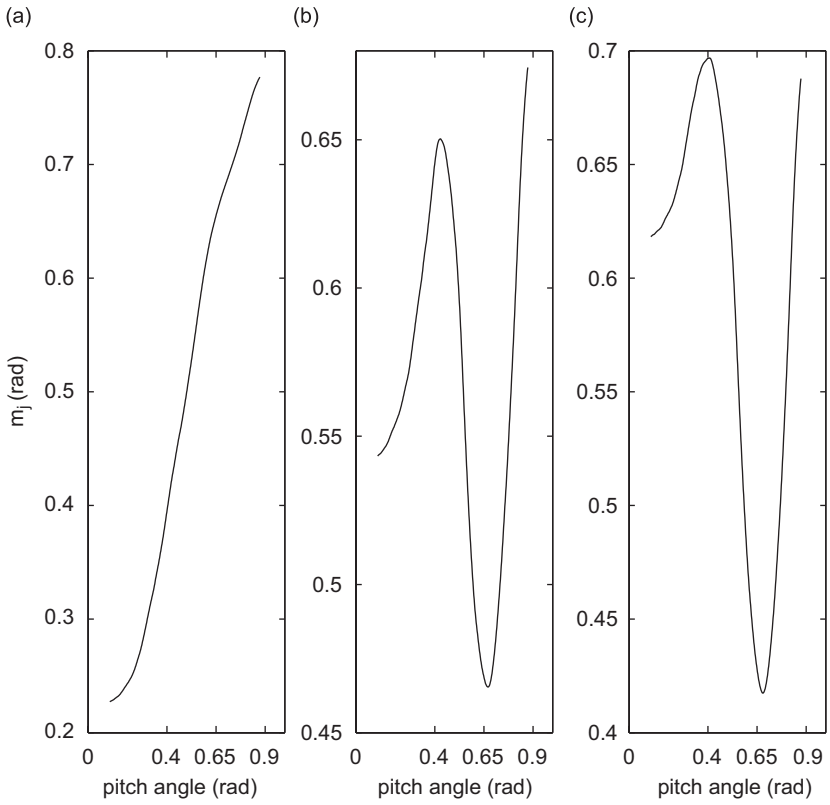

Fig. 4. The estimates of the means for simulated data: (a) $j = -4$, (b) $j = -18$ and (c) $j = -22$.

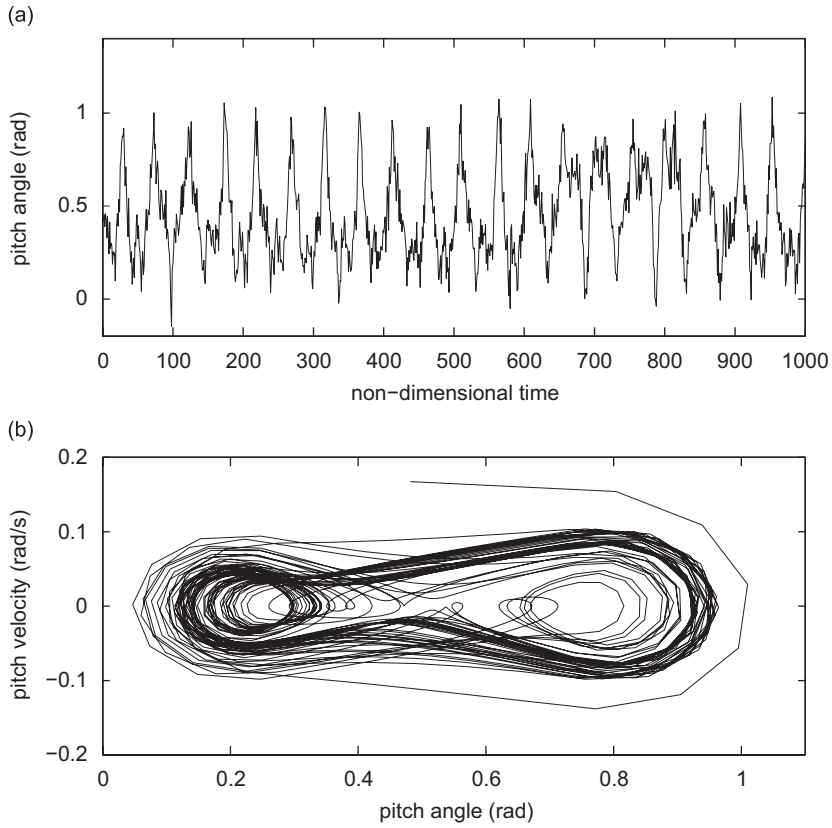

Fig. 5. Simulated chaotic pitch motion: (a) noisy time history for pitch and (b) the phase path α–α' for the simulated clean signal.

and $\alpha_f + \delta = 0.75$. Thus, the complex chaotic dynamics and the presence of a large amount of noise do not affect the performance of the non-parametric method.

The non-parametric method has also been applied to data obtained from experiments. In Fig. 7, we display the mean plots corresponding to experimental freeplay data with $\delta = 1.45$ degrees obtained from McGill University. The estimated switching points are located at $\alpha_f = -1$ and $\alpha_f + \delta = 1$ approximately. Thus, the estimated $\hat{\delta}$ is 2 degrees. For two other sets of experimental data with freeplay with $\delta = 0.64$ and 0.25 degree, we obtain the estimated $\hat{\delta}$ to be 1 and 0.4 degree, respectively. The non-parametric method usually gives less accurate predictions of the freeplay parameters for wind-tunnel tests data than for numerically simulated data. In numerical simulations noise is added to the pitch and plunge signals, but in experiments the noise and the signals cannot be separated. However, in the following we will show that the system identification is not very sensitive to the error in $\hat{\delta}$, and accurate predictions can still be obtained regardless whether the data is generated from experiments or numerical simulations.

Once the presence of a freeplay is confirmed and the locations of the switching points are estimated, the EM algorithm is used to estimate the parameters of the switching state-space model given in Eq. (18). Then, the aeroelastic response is predicted using the reconstructed switching model.

The available transient data are divided into a training and a test set. The training set is used for estimating the parameters, and the test set is used for checking the accuracy of the predictions. From our experience, the number of observations that need to be included in the training set depends on the given signal, and the number of parameters to be estimated. To obtain accurate estimations and predictions, the training set should be formed using the majority of the available observations, so that the main features of the given transient signal are included. For example, a training set formed only by a part of the observations corresponding to one oscillation, or by observations with constant values, will not be appropriate. The fast convergence of the EM algorithm, the substantial increase in the estimated value of the likelihood, and the small one-step

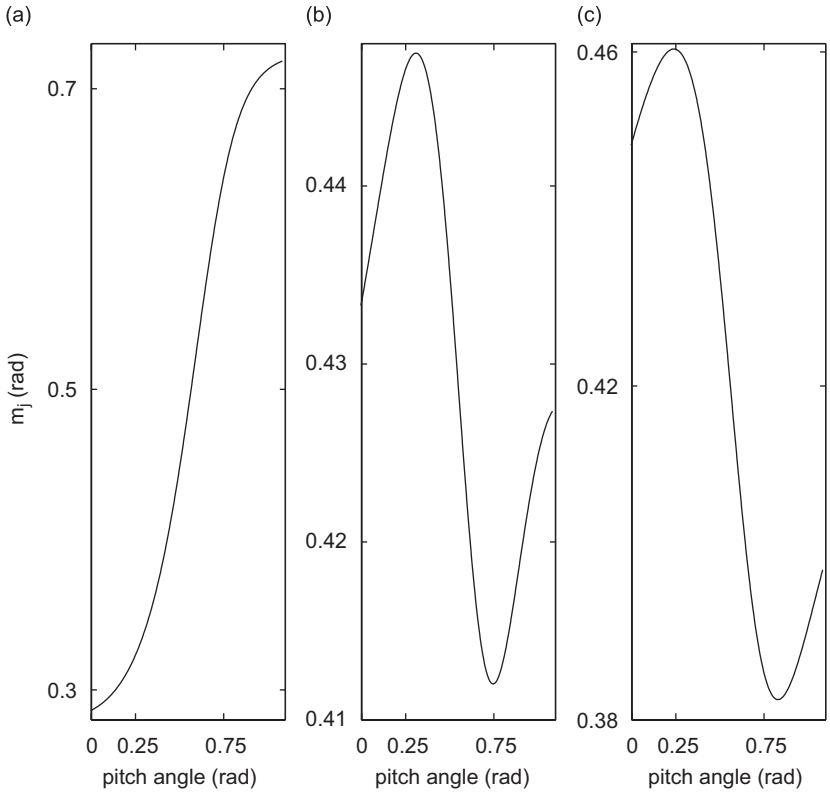

Fig. 6. The estimates of the means for chaotic data: (a) $j=-4$, (b) $j=-11$ and (c) $j=-12$.

prediction errors, all point to the fact that the estimated model will give a good fit for the data. However, the accuracy of the results obtained for the test set is the best measure of the confidence we should have on the estimated model and the predicted steady-state aeroelastic response. Without using a full cross-validation procedure, we have tried several training sets, with increasing number of points or using different time segments of the given transient data. Once the training set becomes large enough, the results should be consistent when comparing the predicted signals.

In this paper, results of three case studies are reported. The first two data sets are from wind-tunnel tests carried out at McGill University, and the third data set is from a numerical simulation using the model given in Eqs. (1) and (2).

For the first signal shown in Fig. 2a, the amplitude of the first few cycles of the input data is increasing. Based on these data, one could not conclude whether the future time series will diverge or will reach a limit cycle oscillation. However, the ES predictions (dashed lines) are in an excellent agreement with the experimental data (solid lines) in terms of the amplitude and frequency of the LCOs, as shown in Fig. 8. The input data are taken from $k=91$ to $k=240$, and are separated by the two vertical lines in Fig. 8 (the time axis in Fig. 2a has been shifted, and $k=1$ corresponds to $k=91$ in Fig. 8). In Fig. 9, we illustrate the convergence of the parameter estimation method by plotting the log-likelihood versus the number of cycles used in the EM algorithm. A very rapid convergence is achieved at the beginning, followed by a slow improvement as more EM steps are applied. This is a typical characteristic of the EM algorithm [21]. In practice, the EM algorithm is terminated when the improvement in the log-likelihood becomes small. For this particular case, we stopped the EM algorithm after 15 cycles. We note that accurate predictions are obtained even though the switching state-space model is not using the exact locations of the switching points, because the estimated $\hat{\delta}$ is 2 degrees, but the correct δ is 1.45 degrees.

The second set of experimental data displayed in Fig. 10 has a more complex behavior. Using the non-parametric method, we confirm the freeplay model with the estimated switching points at $\alpha_f=-0.2$ and

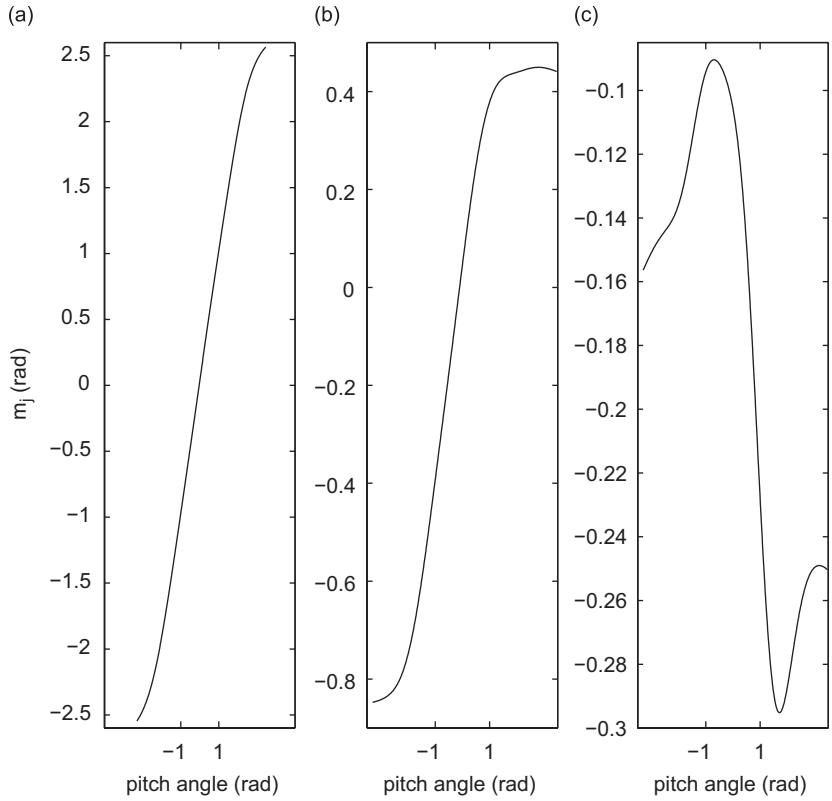

Fig. 7. The estimates of the means for experimental data: (a) $j=-4$, (b) $j=-10$ and (c) $j=-12$.

$\alpha_f+\delta=0.05$. To better illustrate the effectiveness of the proposed ES, we consider two different input data sets using two different segments of the time series.

The first data set corresponds to $k=86$ to $k=260$, as indicated by the two vertical lines in Fig. 10 (see also Fig. 2b which shows the first six cycles of data with time axis shifted such that $k=1$ corresponds to $k=86$ in Fig. 10). Based on the profiles given by these input data for the pitch and plunge motions, it is not possible to predict that the subsequent aeroelastic responses are represented by oscillations with almost constant amplitude, and then followed by a sharp decay to steady-state non-oscillating solutions. In Fig. 10, we compare the experimental data (solid lines) with the results (dashed line) obtained using 56 cycles of the EM algorithm to estimate the system parameters. The agreement is remarkable, we have accurate predictions of the short term LCOs, as well as long term non-oscillating steady-state behavior. However, the steady solutions appear around $k=500$ instead of $k=750$ as recorded from the experiment.

The second data are taken from $k=301$ to $k=475$, as shown by the two vertical lines in Fig. 11. The input pitch and plunge are in LCO regions (see also Fig. 2c with the time axis shifted such that $k=1$ corresponds to $k=301$ in Fig. 11). After applying 36 cycles of the EM algorithm, we obtain the predicted responses (dashed line) shown in Fig. 11. They are in excellent agreement with the experimental results plotted with solid lines, and they show the rapid change from LCO to non-oscillating behavior.

We also consider a set of input data generated by numerical simulation. Using the signal displayed in Fig. 2d as training set, we obtain the predicted response plotted with dashed lines as shown in Fig. 12 (the time axis is shifted and $k=1$ in Fig. 2d corresponds to $k=66$ in Fig. 12). Even though the initial three cycles (shown by two vertical lines in Fig. 12) appear to behave like LCOs, the ES accurately predicts a divergent response.

The previous three sets of data correspond to steady-state responses represented by LCOs, constant amplitude non-oscillating signals and divergent signals. Both the non-parametric method and the EM

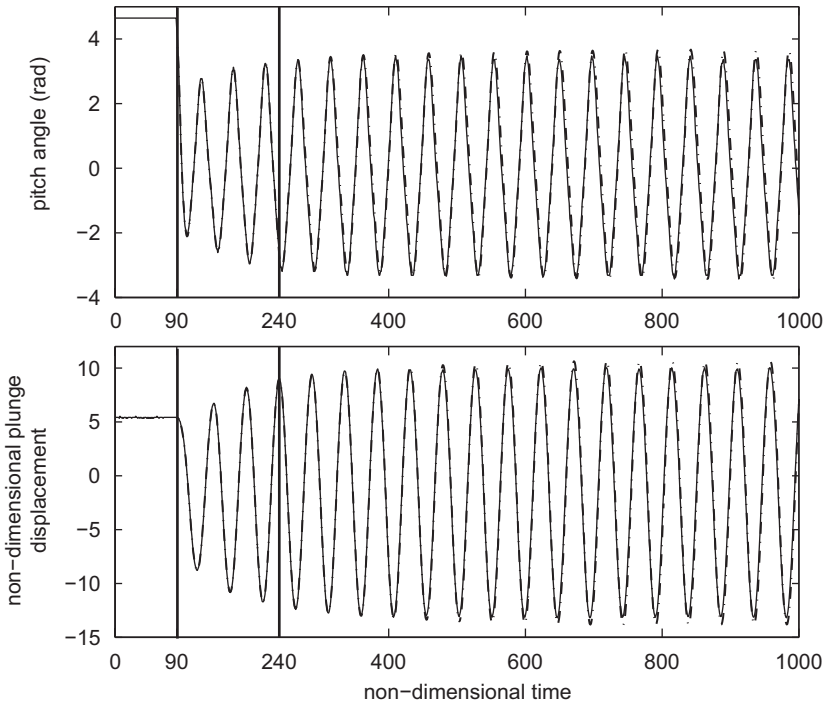

Fig. 8. Limit cycle oscillations: experimental (solid) and predicted (dashed) responses.

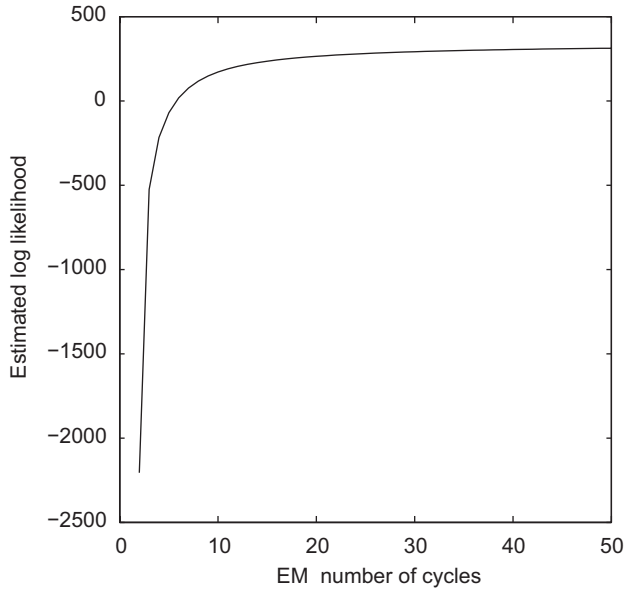

Fig. 9. The convergence of the EM algorithm.

algorithm give very good results for these data. Moreover, we have successfully applied the non-parametric method also for the chaotic data displayed in Fig. 5a. Chaotic motion by definition implies that the dynamic behavior is highly sensitive to the initial conditions, in which a small perturbation in the initial condition could lead to significant changes in the future behavior. Hence, it may not be meaningful to expect that the expert system can accurately predict the future time history of a chaotic motion using a limit transient data as input.

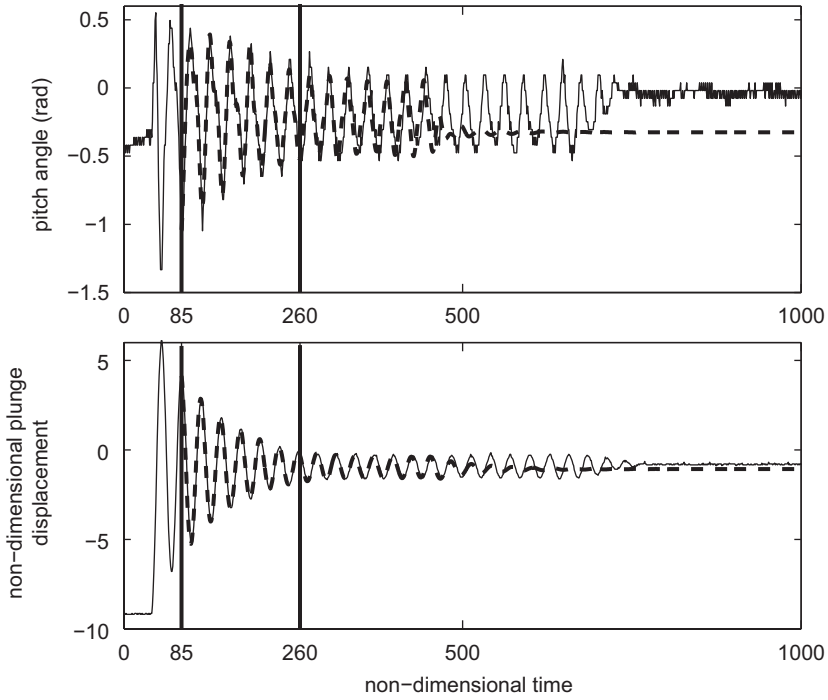

Fig. 10. Damped signals I: experimental (solid) and predicted (dashed) responses.

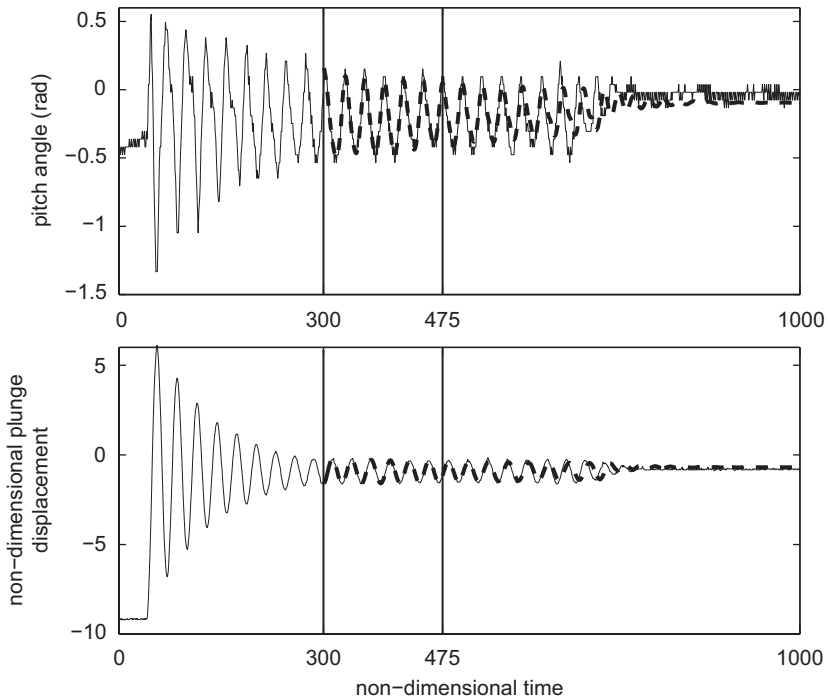

Fig. 11. Damped signals II: experimental (solid) and predicted (dashed) responses.

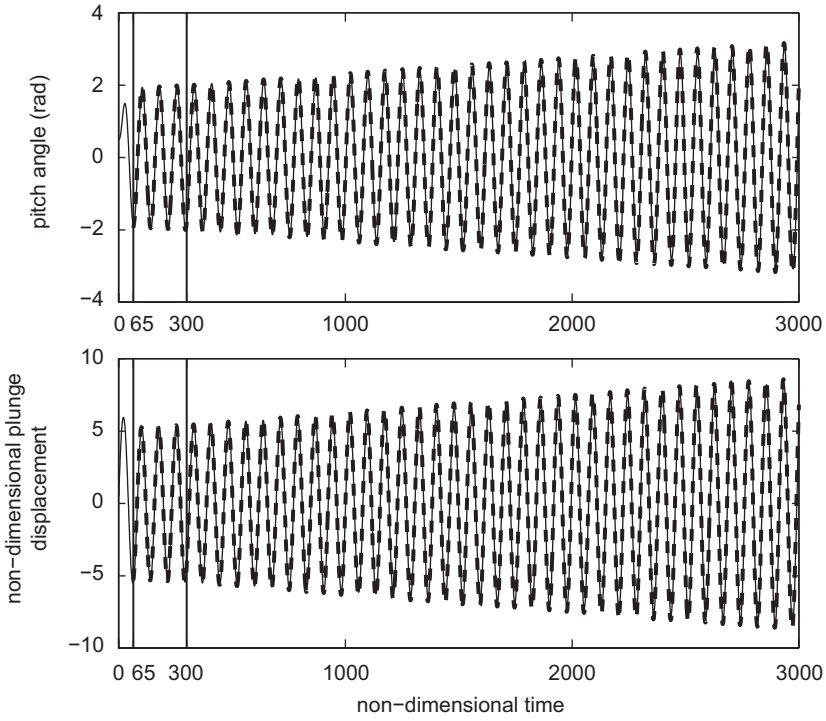

Fig. 12. Divergent motions: experimental (solid) and predicted (dashed) responses.

However, the EM algorithm and the Kalman filter can still be applied for filtering noisy chaotic data. Currently, we are working on some alternative techniques for studying chaotic data.

6. Conclusions

An expert system is developed to predict steady-state nonlinear aeroelastic behavior. The study focuses on aeroelastic data arising from a two-dimensional airfoil oscillating in pitch and plunge, and the source of the structural nonlinearity is due to freeplay in the pitch dof. The success of the ES requires the parameters of the freeplay structural nonlinearity to be determined first. Consequently, a linear system identification technique is effectively applied to reconstruct the switching state-space aeroelastic system.

The ES is tested on short duration transient data generated from experiments and numerical simulations. The examples considered are chosen so that deducing long term behavior from observation of the input time series is not possible or reliable. In all cases, the ES correctly predict the steady-state responses including LCOs, divergent oscillations and constant non-oscillating solutions. The technique has been validated from a number of test cases, and our overall assessment is that the present data driven expert system is a useful tool in the study of nonlinear aeroelasticity. The present formulation is capable to accurately predict the steady-state behavior for an aeroelastic system with freeplay in situations where only short duration transient data are available and long term behavior is required. It is straightforward to extend this method to aeroelastic data with hysteresis nonlinearity. It will be of interest to investigate the performance when the input data is generated from a system subject to both nonlinear aerodynamic forces and structural nonlinearities.

Acknowledgments

The authors would like to thank Dr. C. Marsden of McGill University, and Dr. L. Liu of University of Texas—Pan American for providing the aeroelastic response data sets in our study. The authors would also

like to acknowledge the support received from the Natural Sciences and Engineering Research Council of Canada.

Appendix A. Updating formulas for the EM algorithm

The complete log-likelihood is given by

$$\begin{aligned}\log(L) = {} & \log P(\mathbf{x}_1,\ldots,\mathbf{x}_N,\mathbf{y}_1,\ldots,\mathbf{y}_N,S_1,\ldots,S_N) = \log P(\mathbf{y}_N|\mathbf{y}_{N-1},\ldots,\mathbf{y}_1,\\ & \mathbf{x}_N,\ldots,\mathbf{x}_1,S_N,\ldots,S_1)+\cdots+\log P(\mathbf{y}_1|\mathbf{x}_N,\ldots,\mathbf{x}_1,S_N,\ldots,S_1)+\log P(\mathbf{x}_N|\\ & \mathbf{x}_{N-1},\ldots,\mathbf{x}_1,S_N,\ldots,S_1)+\cdots+\log P(\mathbf{x}_1|S_N,\ldots,S_1)+\log P(S_N,\ldots,S_1).\end{aligned}$$

Using Eq. (18) we obtain

$$\begin{aligned}\log(L) = {} & -5N\ln(2\pi)-\frac{1}{2}\sum_{n=1}^{N}\ln(\det(\mathbf{R}))-\frac{1}{2}\sum_{n=1}^{N}(\mathbf{y}_n-\mathbf{C}\mathbf{x}_n)^{\mathrm{T}}\mathbf{R}^{-1}(\mathbf{y}_n-\mathbf{C}\mathbf{x}_n)\\ & -\frac{1}{2}\sum_{n=2}^{N}\ln(\det(\mathbf{Q}_{S_n}))-\frac{1}{2}\sum_{n=2}^{N}(\mathbf{x}_n-\mathbf{A}_{S_n}\mathbf{x}_{n-1}-\mathbf{b}_{S_n})^{\mathrm{T}}\mathbf{Q}_{S_n}^{-1}(\mathbf{x}_n-\mathbf{A}_{S_n}\mathbf{x}_{n-1}-\mathbf{b}_{S_n})\\ & -\frac{1}{2}\ln(\det(\mathbf{\Sigma}_{S_1}))-\frac{1}{2}(\mathbf{x}_1-\boldsymbol{\mu}_{S_1})^{\mathrm{T}}\mathbf{\Sigma}_{S_1}^{-1}(\mathbf{x}_1-\boldsymbol{\mu}_{S_1})+\log P(S_N,\ldots,S_1).\end{aligned}\tag{21}$$

Let tr denote the trace of a matrix. Then using the previous formulas and $\mathrm{tr}(\mathbf{AB})=\mathrm{tr}(\mathbf{BA})$, we can calculate $\hat{E}=E[\log(L)|\mathbf{y}_1,\ldots,\mathbf{y}_N,S_1=i_1,\ldots,S_N=i_N]$:

$$\begin{aligned}\hat{E} = {} & -5N\ln(2\pi)-\frac{N}{2}\ln(\det(\mathbf{R}))-\frac{1}{2}\sum_{n=1}^{N}\mathrm{tr}[\mathbf{R}^{-1}(\mathbf{y}_n\mathbf{y}_n^{\mathrm{T}}-\mathbf{y}_n\mathbf{x}_{n|N}^{\mathrm{T}}\mathbf{C}^{\mathrm{T}}\\ & -\mathbf{C}\mathbf{x}_{n|N}\mathbf{y}_n^{\mathrm{T}}+\mathbf{C}\mathbf{P}_n\mathbf{C}^{\mathrm{T}})]-\frac{1}{2}\sum_{n=2}^{N}\ln(\det(\mathbf{Q}_{i_n}))-\frac{1}{2}\sum_{n=2}^{N}\mathrm{tr}[\mathbf{Q}_{i_n}^{-1}(\mathbf{P}_n-\mathbf{A}_{i_n}\mathbf{P}_{n,n-1}^{\mathrm{T}}\\ & -\mathbf{P}_{n,n-1}\mathbf{A}_{i_n}^{\mathrm{T}}+\mathbf{A}_{i_n}\mathbf{P}_{n-1}\mathbf{A}_{i_n}^{\mathrm{T}}-\mathbf{x}_{n|N}\mathbf{b}_{i_n}^{\mathrm{T}}-\mathbf{b}_{i_n}\mathbf{x}_{n|N}^{\mathrm{T}}+\mathbf{A}_{i_n}\mathbf{x}_{n-1|N}\mathbf{b}_{i_n}^{\mathrm{T}}\\ & +\mathbf{b}_{i_n}\mathbf{x}_{n-1|N}^{\mathrm{T}}\mathbf{A}_{i_n}^{\mathrm{T}}+\mathbf{b}_{i_n}\mathbf{b}_{i_n}^{\mathrm{T}})]-\frac{1}{2}\ln(\det(\mathbf{\Sigma}_{i_1}))-\frac{1}{2}\mathrm{tr}[\mathbf{\Sigma}_{i_1}^{-1}(\mathbf{P}_1-\boldsymbol{\mu}_{i_1}\mathbf{x}_{1|N}^{\mathrm{T}}-\mathbf{x}_{1|N}\boldsymbol{\mu}_{i_1}^{\mathrm{T}}+\boldsymbol{\mu}_{i_1}\boldsymbol{\mu}_{i_1}^{\mathrm{T}})].\end{aligned}\tag{22}$$

Taking the derivatives with respect to the parameters θ in the previous formula for $\hat{E}$, we derive the updating equations for the parameters [16] from the k-step to the $k+1$-step:

$$\begin{aligned}\mathbf{A}_1(k+1) = {} & \left[\left(\sum_{n=2}^{N}1_{\{1,3\}}(S_n)\mathbf{P}_{n,n-1}\right)\left(\sum_{n=2}^{N}1_{\{1\}}(S_n)\right)\left(\sum_{n=2}^{N}1_{\{3\}}(S_n)\right)\right.\\ & -\left(\sum_{n=2}^{N}1_{\{1\}}(S_n)\mathbf{x}_{n|N}\right)\left(\sum_{n=2}^{N}1_{\{1\}}(S_n)\mathbf{x}_{n-1|N}^{\mathrm{T}}\right)\left(\sum_{n=2}^{N}1_{\{3\}}(S_n)\right)-\left(\sum_{n=2}^{N}1_{\{1\}}(S_n)\right)\\ & \left.\times\left(\sum_{n=2}^{N}1_{\{3\}}(S_n)\mathbf{x}_{n|N}\right)\left(\sum_{n=2}^{N}1_{\{3\}}(S_n)\mathbf{x}_{n-1|N}^{\mathrm{T}}\right)\right]\left[\left(\sum_{n=2}^{N}1_{\{1,3\}}(S_n)\mathbf{P}_{n-1}\right)\right.\\ & \times\left(\sum_{n=2}^{N}1_{\{1\}}(S_n)\right)\left(\sum_{n=2}^{N}1_{\{3\}}(S_n)\right)-\left(\sum_{n=2}^{N}1_{\{1\}}(S_n)\mathbf{x}_{n-1|N}\right)\left(\sum_{n=2}^{N}1_{\{1\}}(S_n)\mathbf{x}_{n-1|N}^{\mathrm{T}}\right)\\ & \left.\times\left(\sum_{n=2}^{N}1_{\{3\}}(S_n)\right)-\left(\sum_{n=2}^{N}1_{\{3\}}(S_n)\mathbf{x}_{n-1|N}\right)\left(\sum_{n=2}^{N}1_{\{1\}}(S_n)\right)\left(\sum_{n=2}^{N}1_{\{3\}}(S_n)\mathbf{x}_{n-1|N}^{\mathrm{T}}\right)\right]^{-1},\end{aligned}\tag{23}$$

$$\mathbf{A}_2(k+1)=\left[\left(\sum_{n=2}^{N}1_{\{2\}}(S_n)\mathbf{P}_{n,n-1}\right)\left(\sum_{n=2}^{N}1_{\{2\}}(S_n)\right)-\left(\sum_{n=2}^{N}1_{\{2\}}(S_n)\mathbf{x}_{n-1|N}^{\mathrm{T}}\right)\times\left(\sum_{n=2}^{N}1_{\{2\}}(S_n)\mathbf{x}_{n|N}\right)\right]\left[\left(\sum_{n=2}^{N}1_{\{2\}}(S_n)\mathbf{P}_{n-1}\right)\left(\sum_{n=2}^{N}1_{\{2\}}(S_n)\right)-\left(\sum_{n=2}^{N}1_{\{2\}}(S_n)\mathbf{x}_{n-1|N}\right)\left(\sum_{n=2}^{N}1_{\{2\}}(S_n)\mathbf{x}_{n-1|N}^{\mathrm{T}}\right)\right]^{-1},\tag{24}$$

$$\mathbf{b}_i(k+1)=\left[\sum_{n=2}^{N}1_{\{i\}}(S_n)(\mathbf{x}_{n|N}-\mathbf{A}_i(k+1)\mathbf{x}_{n-1|N})\right]\Big/\sum_{n=2}^{N}1_{\{i\}}(S_n),\tag{25}$$

$$\mathbf{R}(k+1)=\left(\sum_{n=1}^{N}\mathbf{y}_n\mathbf{y}_n^{\mathrm{T}}-\mathbf{C}\sum_{n=1}^{N}\mathbf{x}_{n|N}\mathbf{y}_n^{\mathrm{T}}-\sum_{n=1}^{N}\mathbf{y}_n\mathbf{x}_{n|N}^{\mathrm{T}}\mathbf{C}^{\mathrm{T}}+\mathbf{C}\left(\sum_{n=1}^{N}\mathbf{P}_n\right)\mathbf{C}^{\mathrm{T}}\right)\Big/N,\tag{26}$$

$$\mathbf{Q}_i(k+1)=\left[\sum_{n=2}^{N}1_{\{i\}}(S_n)(\mathbf{P}_n-\mathbf{A}_i(k+1)\mathbf{P}_{n,n-1}^{\mathrm{T}}-\mathbf{b}_i(k+1)\mathbf{x}_{n-1|N}^{\mathrm{T}})\right]\Big/\sum_{n=2}^{N}1_{\{i\}}(S_n),\tag{27}$$

$$\boldsymbol{\mu}_i(k+1)=\mathbf{x}_{1|N},\quad \boldsymbol{\Sigma}_i(k+1)=\mathbf{P}_1-\mathbf{x}_{1|N}\mathbf{x}_{1|N}^{\mathrm{T}}.\tag{28}$$

Here $i=1,2,3$, $\mathbf{A}_3(k+1)=\mathbf{A}_1(k+1)$, and 1_Ω denotes the characteristic function of the set Ω.

References

[1] E. Dowell, J.W. Edwards, T. Strganac, Nonlinear aeroelasticity, *Journal of Aircraft* 40 (2003) 857–874.

[2] Y. Wong, O. Voitcu, C. Popescu, An expert data mining system for nonlinear aeroelastic response prediction, *Proceedings of the International Council of the Aeronautical Sciences Congress*, Toronto, ON, Canada, 2002.

[3] C.A. Popescu, Y.S. Wong, A nonlinear statistical approach for aeroelastic response prediction, *AIAA Journal of Guidance, Control, and Dynamics* 26 (4) (2003) 565–572.

[4] G. Vio, G. Dimitriadis, J. Cooper, K. Badcock, M. Woodgate, A. Rampurawala, Aeroelastic system identification using transonic CFD data for a wing/store configuration, *Aerospace Science and Technology* 11 (5) (2007) 146–154.

[5] C.A. Popescu, Y.S. Wong, Intelligent identification system with applications to transient aeroelastic data, *Proceedings of the 48th AIAA/ASME/ASCE/AHS/ASC/Structures, Structural Dynamics, and Materials Conference*, Honolulu, HI, USA, 2007, AIAA Paper 2007-1773.

[6] M. Hajj, W.A. Silva, Nonlinear flutter aspects of the flexible high-speed civil transport semispan model, *Journal of Aircraft* 41 (2004) 1202–1208.

[7] W.A. Silva, T.W. Strganac, M.R. Hajj, Higher-order spectral analysis of a nonlinear pitch and plunge apparatus, *Proceedings of the 46th AIAA/ASME/ASCE/AHS/ASC/Structures, Structural Dynamics, and Materials Conference*, Austin, TX, USA, 2005, AIAA Paper 2005-2013.

[8] W.A. Silva, S. Dunn, Higher order spectral analysis of F-18 flight flutter data, *Proceedings of the 46th AIAA/ASME/ASCE/AHS/ASC/Structures, Structural Dynamics, and Materials Conference*, Austin, TX, USA, 2005, AIAA Paper 2005-2014.

[9] C.C. Chabalko, M.R. Hajj, D.T. Mook, W.A. Silva, Characterization of the LCO response behaviors of the NATA model, *Proceedings of the 47th AIAA/ASME/ASCE/AHS/ASC/Structures, Structural Dynamics, and Materials Conference*, Newport, RI, USA, 2006, AIAA Paper 2006-1852.

[10] B.H.K. Lee, S.J. Price, Y.S. Wong, Nonlinear aeroelastic analysis of airfoils: bifurcation and chaos, *Progress in Aerospace Sciences* 35 (1999) 205–334.

[11] W. Hardle, *Applied Nonparametric Regression*, Cambridge University Press, New York, 1990.

[12] J.S. Marron, D. Nolan, Canonical kernels for density estimation, *Statistics & Probability Letters* 7 (1989) 195–199.

[13] R. Tsay, *Analysis of Financial Time Series*, Wiley, New York, 2002.

[14] H. Tong, *Nonlinear Time Series*, The Clarendon Press, Oxford University Press, New York, 1990.

[15] R. Neal, G. Hinton, A view of the EM algorithm that justifies incremental, sparse, an other variants, in: M. Jordan (Ed.), *Learning in Graphical Models*, 1998.

[16] R. Shumway, D. Stoffer, An approach to time series smoothing and forecasting using the EM algorithm, *Journal of Time Series Analysis* 3 (4) (1982) 253–264.

[17] Z. Ghahramani, S. Roweis, Learning nonlinear dynamical systems using an EM algorithm, in: M. Kearns, S. Solla, C.D.A. (Eds.), *Advances in Neural Information Processing Systems*, MIT Press, Cambridge, MA, 1999, pp. 599–605.
[18] E.A. Wan, R. Van der Merwe, A. T. Nelson, Dual estimation and the unscented transformation, in: J.S. Bolton, P. Davies (Eds.), Advances in Neural Information Processing Systems, MIT Press, 2000.
[19] C. Wu, On the convergence properties of the EM algorithm, *The Annals of Statistics* 11 (1) (1983) 95–103.
[20] C. Biernacki, G. Celeux, G. Govaert, Choosing starting values for the EM algorithm for getting the highest likelihood in multivariate gaussian mixture models, *Computational Statistics & Data Analysis* 41 (2003) 561–575.
[21] X. Meng, D. Van Dyk, The EM algorithm—an old folk-song to a fast new tune, *Journal of the Royal Statistical Society: Series B* 59 (3) (1997) 511–567.
[22] L. Liu, E. Dowell, Harmonic balance approach for an airfoil with a freeplay control surface, *AIAA Journal* 43 (2005) 802–815.
[23] C.A. Popescu, Y.S. Wong, B.H.K. Lee, System identification for nonlinear aeroelastic models, *Proceedings of the 46th AIAA/ASME/ASCE/AHS/ASC/Structures, Structural Dynamics, and Materials Conference*, Austin, TX, USA, 2005, AIAA Paper 2005-1855.
[24] S. Price, H. Alighambari, B. Lee, The aeroelastic response of a two-dimensional airfoil with bilinear and cubic structural nonlinearities, *Journal of Fluids and Structures* 9 (1995) 175–193.